

# Scalable Synthesis and Characterization of Multilayer $\gamma$ -Graphyne, New Carbon Crystals with a Small Direct Band Gap

Victor G. Desyatkin,<sup>▽</sup> William B. Martin,<sup>▽</sup> Ali E. Aliev, Nathaniel E. Chapman, Alexandre F. Fonseca, Douglas S. Galvão, Ericka Roy Miller, Kevin H. Stone, Zhong Wang, Dante Zakhidov, F. Ted Limpoco, Sarah R. Almahdali, Shane M. Parker, Ray H. Baughman, and Valentin O. Rodionov<sup>\*</sup>



Cite This: *J. Am. Chem. Soc.* 2022, 144, 17999–18008



Read Online

ACCESS |



Metrics & More

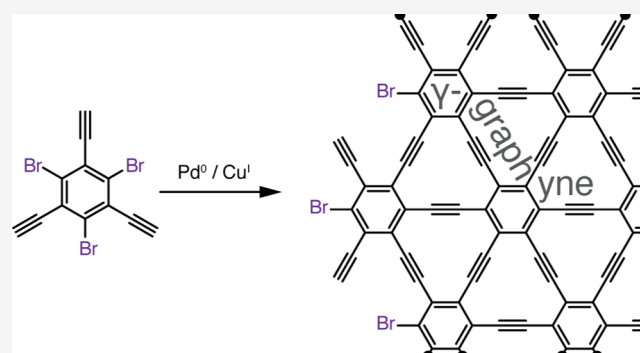


Article Recommendations



Supporting Information

**ABSTRACT:**  $\gamma$ -Graphyne is the most symmetric  $sp^2/sp^1$  allotrope of carbon, which can be viewed as graphene uniformly expanded through the insertion of two-carbon acetylenic units between all the aromatic rings. To date, synthesis of bulk  $\gamma$ -graphyne has remained a challenge. We here report the synthesis of multilayer  $\gamma$ -graphyne through crystallization-assisted irreversible cross-coupling polymerization. A comprehensive characterization of this new carbon phase is described, including synchrotron powder X-ray diffraction, electron diffraction, lateral force microscopy, Raman spectroscopy, infrared spectroscopy, and cyclic voltammetry. Experiments indicate that  $\gamma$ -graphyne is a 0.48 eV band gap semiconductor, with a hexagonal  $a$ -axis spacing of 6.88 Å and an interlayer spacing of 3.48 Å, which is consistent with theoretical predictions. The observed crystal structure has an aperiodic sheet stacking. The material is thermally stable up to 240 °C but undergoes transformation at higher temperatures. While conventional 2D polymerization and reticular chemistry rely on error correction through reversibility, we demonstrate that a periodic covalent lattice can be synthesized under purely kinetic control. The reported methodology is scalable and inspires extension to other allotropes of the graphyne family.



## INTRODUCTION

Over five hundred carbon phases have been theoretically predicted, but few have been experimentally realized.<sup>1</sup> Allotropes based on the hexagonal lattices of  $sp^2$ -hybridized carbons, including few-layer graphene,<sup>2</sup> nanotubes,<sup>3</sup> and fullerenes,<sup>4</sup> are synthetically accessible at scale. These materials have been revolutionary for fundamental physics and materials science and found applications in post-silicon electronics, high-capacity batteries, organic solar cells, extreme-strength composites, and other fields.

In contrast, advances in the synthesis of nonbenzenoid carbon allotropes have been limited. Several  $sp^2$ -based nanographenes with non-hexagonal rings,<sup>5,6</sup> as well as an extended nonbenzenoid biphenylene network,<sup>7</sup> were described. Materials containing  $sp^1$ -hybridized linear arrangements remain even more elusive. Linear polyyne chains  $-(C\equiv C)_n-$  are unstable even for moderate chain lengths unless they are stabilized with bulky end-capping groups<sup>8</sup> or confined inside carbon nanotubes.<sup>9</sup> Graphynes, a family of hybrid lattices combining  $sp^1$  and  $sp^2$  carbons, were first theoretically proposed by Baughman, Eckhardt, and Kertesz in 1987.<sup>10</sup> These allotropes can be formally viewed as graphenes that are expanded through the insertion of acetylenic groups. Graphynes are commonly divided into two types: graphynes- $n$  in

which the aromatic rings are separated by  $n$  acetylenic bonds (Figure 1a) and  $x$ ,  $y$ ,  $z$ -graphynes featuring at least some nonaromatic  $sp^2$  carbons (Figure 1b,c). Theoretical studies of some graphyne lattices suggest unique electronic and chemical properties,<sup>11</sup> including an intrinsic band gap and electrochemical capacities that far exceed that of graphite.<sup>12</sup> To date, few-layer graphyne-2 or graphdiyne (Figure 1a,  $n = 2$ ) is the only graphyne family allotrope that has been synthesized (typically at submilligram scale) and thoroughly characterized.<sup>13</sup>

$\gamma$ -Graphyne (Figure 1d), the basic graphyne- $n$  homologue ( $n = 1$ ), is especially intriguing. Single-layer  $\gamma$ -graphyne is predicted to be a semiconductor with a moderate band gap,<sup>14</sup> ultrafast charge carrier mobility comparable to that of graphene,<sup>15</sup> high thermal conductivity,<sup>16</sup> and exceptional strength.<sup>17</sup> Because of these properties,  $\gamma$ -graphyne could form the basis for the next-generation carbon-based devices.  $\gamma$ -

Received: July 14, 2022

Published: September 21, 2022



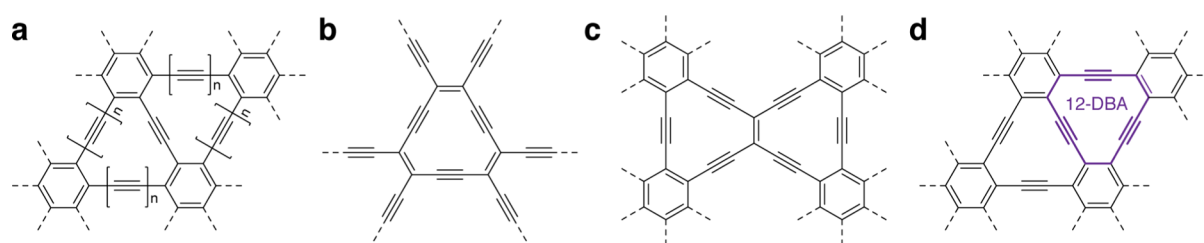


**Figure 1.** Graphyne family allotropes of carbon. (a) Graphynes- $n$  (graphdiyne for  $n = 2$ ). (b) 12,12,12-Graphyne. (c) 6,6,12-Graphyne. (d) Graphyne (or  $\gamma$ -graphyne).

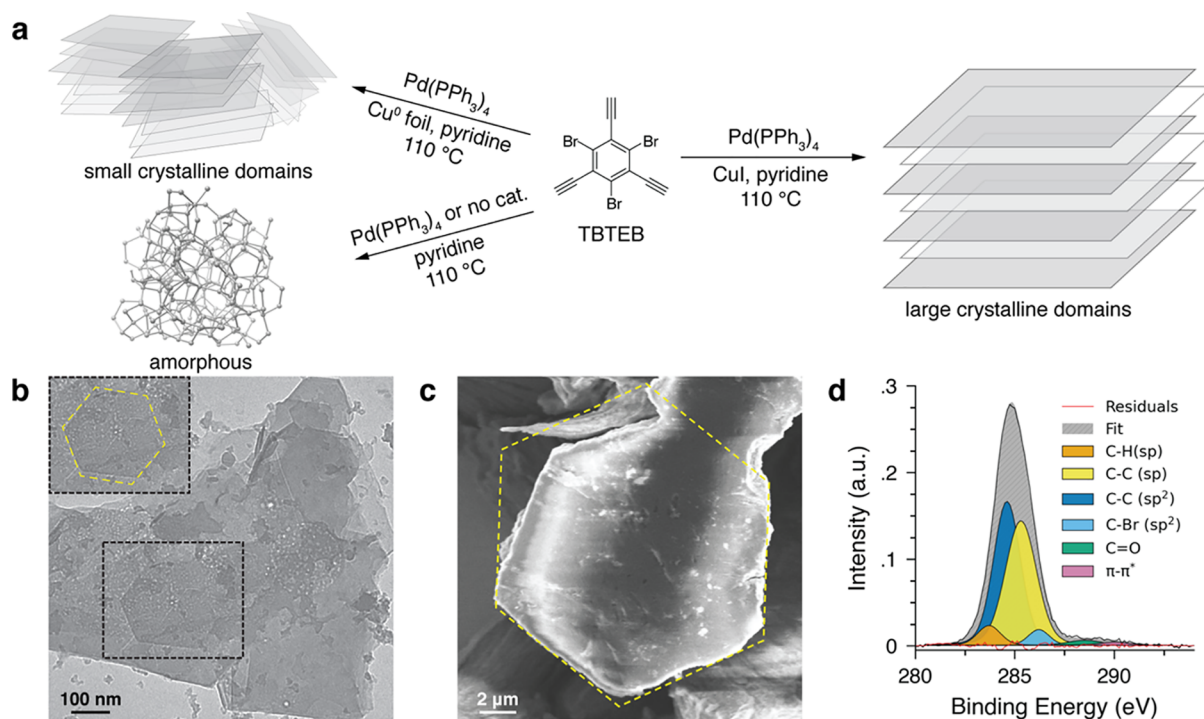


**Figure 2.** Two-dimensional polymerizations of TBTEB. (a) Overview of selected reaction conditions. (b,c) Representative bright-field TEM and SEM images of the carbon flakes obtained from the Pd(PPh<sub>3</sub>)<sub>4</sub>/CuI homogeneous reaction. Inset in (b) emphasizes the hexagonal shape of the layer. (d) High-resolution XPS for the C 1s region of the sample in (b).

Graphyne oligomers containing up to four dehydrobenzo[12]-annulene (12-DBA) repeat units have been prepared through multistep organic synthesis,<sup>18,19</sup> but the synthesis of the extended crystalline lattice remains challenging.

Pyrolytic and vapor deposition methodologies commonly used for the controlled synthesis of benzenoid carbons are unsuitable for sp<sup>1</sup>-based structures, as acetylenes readily convert to graphene or amorphous carbon at elevated temperatures. While graphdiyne<sup>13</sup> and graphdiyne–graphene heterostructures<sup>20</sup> have been synthesized *via* templated solution-phase 2D polymerization, a similar approach has not been previously attempted for  $\gamma$ -graphyne. The reported graphdiyne syntheses rely on the polymerization of highly energetic hexaethynylbenzene through Glaser–Hay sp<sup>1</sup>–sp<sup>1</sup> coupling, which can be conveniently localized at metal surfaces.<sup>21</sup> A comparable synthesis of  $\gamma$ -graphyne would require either coupling between sp<sup>1</sup> and sp<sup>2</sup> carbons or *de novo* formation of three acetylenic bonds per each 12-DBA repeat unit. The most common and general methodology for sp<sup>1</sup>–sp<sup>2</sup> C–C coupling is the Sonogashira reaction.<sup>22</sup> The mechanism of this reaction is thought to involve a homogeneous Pd<sup>0</sup> catalytic cycle, like all other Pd-catalyzed

cross-coupling reactions. Therefore, attempting to confine this chemistry to the surface of a template would be challenging. Moreover, previously reported  $\gamma$ -graphyne oligomers are distorted from planarity, due to steric hindrance introduced by the terminal functionalities.<sup>23</sup> This inevitable distortion, as well as the typically poor solubility of oligomers, limits the stepwise extension of the lattice beyond three to four 12-DBA units.<sup>18</sup>

## RESULTS AND DISCUSSION

Here, we demonstrate that under appropriately adjusted Sonogashira coupling conditions, an A<sub>3</sub>B<sub>3</sub>-type monomer, 1,3,5-tribromo-2,4,6-triethynylbenzene (TBTEB, Figure 2a), can be polymerized into extended  $\gamma$ -graphyne. The main idea that guided our thinking is that an effective route to graphynes and similar rigid 2D polymers could proceed through reactions that create multiple connections in a single step or through a series of kinetically coupled fast steps. Such mechanism would bypass the kinetic dead end of partially connected intermediates, as each monomer unit will “click” into place. Furthermore, this polymerization would be self-correcting. Defects in the growing lattice would be the most reactive sites

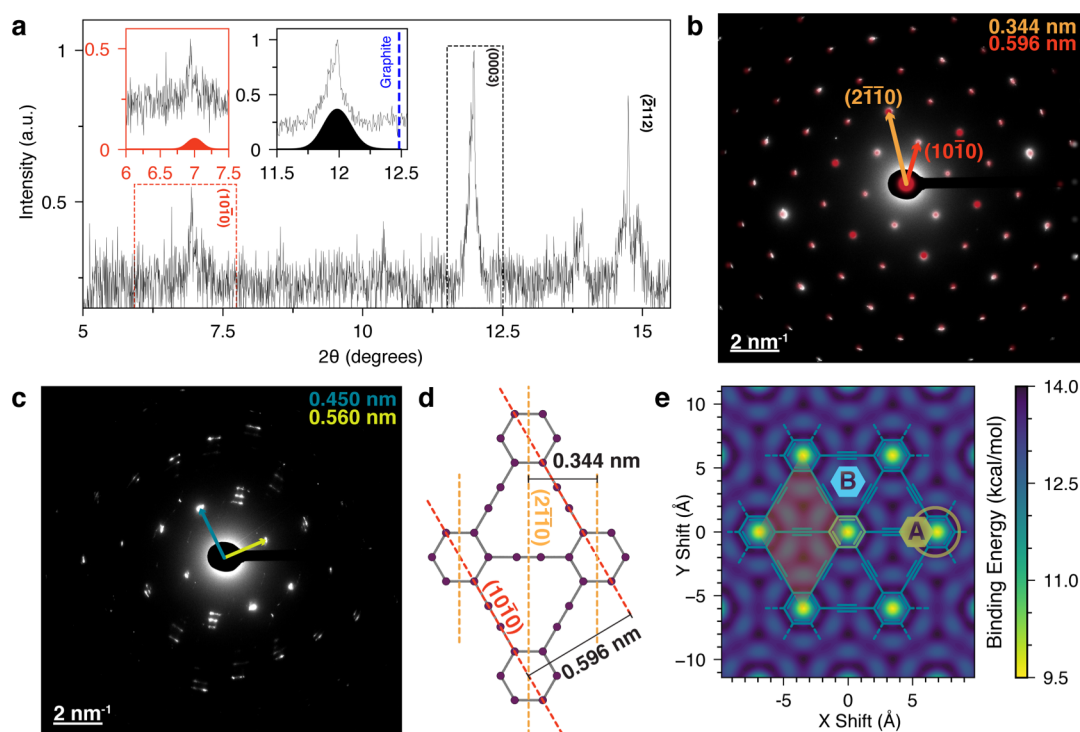


**Figure 3.** X-ray and electron diffraction patterns of  $\gamma$ -graphyne. (a) Synchrotron PXRD pattern (0.728 Å radiation) of  $\gamma$ -graphyne produced by the Pd(PPh<sub>3</sub>)<sub>4</sub>/CuI protocol. Left inset (red): peak at 7.0°  $2\theta$  superimposed with the modeled (1010) peak for  $\gamma$ -graphyne with  $P3_12$  stacking. Right inset (black): peak at 12.0°  $2\theta$  superimposed with the (0003) peak for the same model. The dashed blue line is the (0002) peak center for graphite. (b) Representative SAED pattern (white) of the same material overlaid with the simulated  $c$  orientation diffraction pattern (red) for a structure with no systematic absences. (c) SAED pattern of the sample region in (b), rotated by 45°. (d) DFT-generated model of a  $\gamma$ -graphyne sheet overlaid with crystal planes of interest. (e) DFT-generated potential energy surface for the stacking of two  $\gamma$ -graphyne sheets. The binding energy calculated for a single unit cell (highlighted).

due to local distortions and strain, which could be relieved upon multisite reaction with the monomer. Thus, our two primary aims were to establish reaction conditions favoring exhaustive coupling of the multifunctional TBTEB and to find a way to template the formation of the desired 2D lattice instead of disordered hyperbranched structures.

Several types of Suzuki–Miyaura, Kumada, and Negishi cross-couplings favor exhaustive substitution in multifunctional substrates. This mode of reactivity has previously been exploited for the syntheses of polyfunctional arenes<sup>24</sup> and low-defect hyperbranched polyphenylenes,<sup>25</sup> as well as for pseudo-living chain polymerizations.<sup>26</sup> In all these cases, it is assumed that an exceptionally reactive Pd species is formed after the initial catalytic cycle.<sup>24</sup> The subsequent coupling steps are catalyzed by this Pd species, proceed inside the solvent cage, and are diffusion-controlled. We reasoned that we could extend this reaction mode to Sonogashira-type chemistry. Furthermore, while the nature of the Cu-mediated catalytic cycle in Sonogashira coupling remains largely unexplored, it is broadly understood to involve Cu acetylides.<sup>22</sup> The latter can assume either three-dimensional or low-dimensional polymeric forms<sup>27</sup> or possibly associate with a metal surface. We hypothesized that a Cu surface could template the  $\gamma$ -graphyne lattice, like it presumably does in the reported syntheses of graphdiyne.<sup>13</sup>

We synthesized TBTEB using a known method<sup>28</sup> and screened its reactivity under a range of conditions (Figure 2a and Table S1, Supporting Information). In the control experiment in the absence of catalysts, TBTEB decomposed in refluxing pyridine with a half-life of  $\sim 24$  h, yielding an

amorphous carbonaceous material (Figure S19, Supporting Information). The XPS survey indicated a moderate loss of Br through spontaneous hydrodebromination (Figures S12 and S14d, Supporting Information). A similar featureless carbon was produced in the control experiment with just a Pd precatalyst and no source of Cu (Figure S18, Supporting Information).

Experiments performed in the presence of both Pd and Cu produced outcomes dependent on the state of the metals. Pd(II) precatalysts, as well as PEPPSI-IPr, which we selected for its propensity for multisite coupling,<sup>24</sup> yielded amorphous carbons broadly comparable to the control products. However, for stoichiometric loading of Pd(PPh<sub>3</sub>)<sub>4</sub> in the presence of Cu foil, we obtained a black lustrous material (Figure S15b, Supporting Information). The TEM and SEM images of this material revealed flakes composed of stacks of flat sheets (Figures S17 and S21, Supporting Information). Selected area electron diffraction (SAED) experiments produced dotted ring patterns (Figure S17e,f, Supporting Information), and no Moiré fringes were observed in bright-field TEM, indicating submicron crystalline domains with random orientation.

While the possibility of the layered flakes being a phase of  $\gamma$ -graphyne was intriguing, the data were insufficient to make a structural assignment. XPS survey indicated that the product was primarily carbonaceous but contaminated by Pd, P, and C from the catalyst (Figure S10, Supporting Information). As a multilayered material was obtained, we reasoned that the coupling reaction cannot be confined to the surface of the foil and decided to investigate the sources of Cu other than the metallic surface. To our surprise and delight, reactions

employing soluble CuI also yielded layered flakes (Figures 2b, S15a, and S16, Supporting Information). The crystallinity of this material was significantly improved over the product produced using Cu foil, with Moiré fringes observable in the bright-field TEM images (Figure S16a, Supporting Information). Some of the flakes had well-defined hexagonal shapes (Figures 2b and S16d, Supporting Information). Micron-sized hexagonal prisms with terraces could be observed in the SEM images (Figures 2c and S20d, Supporting Information). A similar hexagonal morphology was previously reported for graphdiyne produced *via* interfacial synthesis.<sup>29</sup>

The higher crystallinity of the product obtained through the optimized homogeneous Pd(PPh<sub>3</sub>)<sub>4</sub>/CuI protocol allowed for a more efficient removal of contaminants. Survey XPS of this product indicated a level of contamination with Pd and P that was below the detection limit of the technique (Figure S9, Supporting Information). We acquired high-resolution XPS data for the C 1s region of this material (Figure 2d), as well as for three controls: the product of the Cu foil synthesis, the Pd-only reaction, and thermal reaction products (Figure S13, Supporting Information). The C 1s peak can be deconvoluted into five subpeaks, corresponding to C–H (terminal alkyne sp<sup>1</sup>),<sup>30</sup> C≡C (internal alkyne sp<sup>1</sup>), C=C (aromatic sp<sup>2</sup>), aromatic C–Br, and C=O carbons.<sup>31</sup> The contribution of C=O is negligible for all samples, indicating little to no oxidation under the reducing/anaerobic reaction conditions. Without the contribution of the sp<sup>1</sup> subpeak, none of the fits converge, which strongly supports the presence of acetylenic bonds in all products. The XPS spectrum indicates a 1:1 ratio of sp<sup>1</sup> to sp<sup>2</sup> carbons in the crystalline material synthesized by the homogeneous Pd(PPh<sub>3</sub>)<sub>4</sub>/CuI protocol, which is consistent with  $\gamma$ -graphyne. This ratio is much higher in the control samples (Figure S13b–d, Supporting Information), due to the extensive side reactions and contamination with aromatic impurities. The  $\pi$ – $\pi^*$  “shake-up” peak at 290 eV is commonly observed in the XPS spectra of graphitic carbons and graphene, as well as small aromatic molecules.<sup>31</sup> Notably, this peak does not appear in the XPS spectrum of graphdiyne.<sup>20</sup> The “shake-up” feature was negligible for the product of the homogeneous Cu protocol (Figure 2d), strongly suggesting that this material is not graphitic. The peak was prominent for the control products that were also contaminated with P (Figures S10, S11, and S13c,d, Supporting Information), indicating that it may be related to adsorbed PPh<sub>3</sub>.

The initial structural identification of the crystalline carbon material was made *via* synchrotron powder X-ray diffraction (PXRD) using a 0.728 Å wavelength (Figure 3a). We observed a peak at 7.0° 2 $\theta$ , which matches the predicted<sup>11</sup> 5.96 Å spacing between the (10 $\bar{1}$ 0) planes of  $\gamma$ -graphyne (Figure 3a, left inset and Figure 3d). The intense peak at 12.0° 2 $\theta$  could be indexed to the (0003) plane, corresponding to an interlayer distance of 3.48 Å (Figure 3a, right inset). To index the other observed peaks, we explored the possible crystal structures of  $\gamma$ -graphyne. While there is a single stable crystallographic configuration for two graphene sheets, a variety of arrangements are possible for bilayer  $\gamma$ -graphyne. Some of these bilayer stackings have been previously identified.<sup>32</sup> To systematically survey the possible structures, we used density functional theory (DFT) to analyze the potential energy surface for a  $\gamma$ -graphyne bilayer. The computed surface (Figure 3e) is a function of the horizontal offset of the upper  $\gamma$ -graphyne layer relative to the lower layer with a fixed interlayer

distance of 3.35 Å. The chosen interlayer distance was based on the first-pass optimization of the bilayer geometry and is underestimated due to the difficulty of computationally modeling van der Waals interactions.<sup>32</sup> The calculations identified two types of local energy minima: one where the upper layer aromatic rings overlay the 12-DBA rings of the lower layer (Figure 3e, binding site B) and the second one where there is a fixed lateral distance between the centers of the upper and lower layer aromatic rings (Figure 3e, binding site A). The absolute energy minimum of the former arrangement gives rise to a single crystal structure with AB mode of stacking corresponding to the P6<sub>3</sub>mc space group. However, at least six bilayer structures are possible for binding at site A with energy minima that are nearly identical within the error of calculations, giving rise to a multitude of AB, ABC, or more complex arrangements for multiple sheets. To further explore this complex energy map, which would be expensive for DFT calculations, we ran fully atomistic reactive molecular dynamics (MD) simulations for three to six layers of  $\gamma$ -graphyne. In all cases, the simulations converged to stacks of sheets bound exclusively at A sites (Figures S34 and S35, Supporting Information). However, for multiple sheets stacked through A sites, the energy barrier for transitioning between different A site configurations is extremely small, as this energy difference depends upon the van der Waals interactions between nonadjacent graphyne sheets. Modeling indicated that several of the less-ordered stacking modes identified by the MD and DFT calculations produce PXRD patterns that closely match our experimental diffraction patterns. Thus, we could index the peak at 14.5° 2 $\theta$  to the (2112) plane.

We further explored the structure and symmetry of the crystals using electron diffraction. The spot SAED patterns of  $\gamma$ -graphyne produced with the Pd(PPh<sub>3</sub>)<sub>4</sub>/CuI protocol were exceptionally well defined, consistent for different regions of the sample, and independent of the size or presence of a selected area aperture. The near-perfect uniformity of the patterns indicates that the material consists of crystalline domains that are sufficiently large to span the entire illuminated region of our typical imaging frame of 2 × 2  $\mu$ m (Figures 2b and S16, Supporting Information), indicating crystalline domain sizes of at least 1–3  $\mu$ m.<sup>33</sup> The diffraction patterns observed from the flat areas of the sample had perfect hexagonal symmetry (Figure 3b). Using the bond distances calculated by DFT and the interlayer distance obtained from PXRD, we built models for several plausible stacking modes of  $\gamma$ -graphyne. These models were used to simulate electron diffraction in the *c*, *b*, and intermediate crystal orientations that lie  $\sim$ 45° to the (0001) pole (Figure S23, Supporting Information). The simulated *c* orientation patterns exclusively involve spacings in the basal plane (Figure S22c,d, Supporting Information). The first- and second-order reflections in the experimental diffraction pattern correspond to *d*-spacings of 5.96 and 3.44 Å, which perfectly match the theoretically calculated spacings<sup>11</sup> for the (10 $\bar{1}$ 0) and (11 $\bar{2}$ 0) plane sets of  $\gamma$ -graphyne (Figure 3b,d). Both these distances are defined in part by the length of the acetylenic bond. Some of the more symmetric space groups, such as *Cmcm* and *R3m*, are expected to produce diffraction patterns with systematic absences. As there were no such systematic absences in the observed diffraction pattern, these space groups could be conclusively eliminated.

Additional SAED patterns were obtained for an alternate sample orientation. The initial position of the stage was chosen

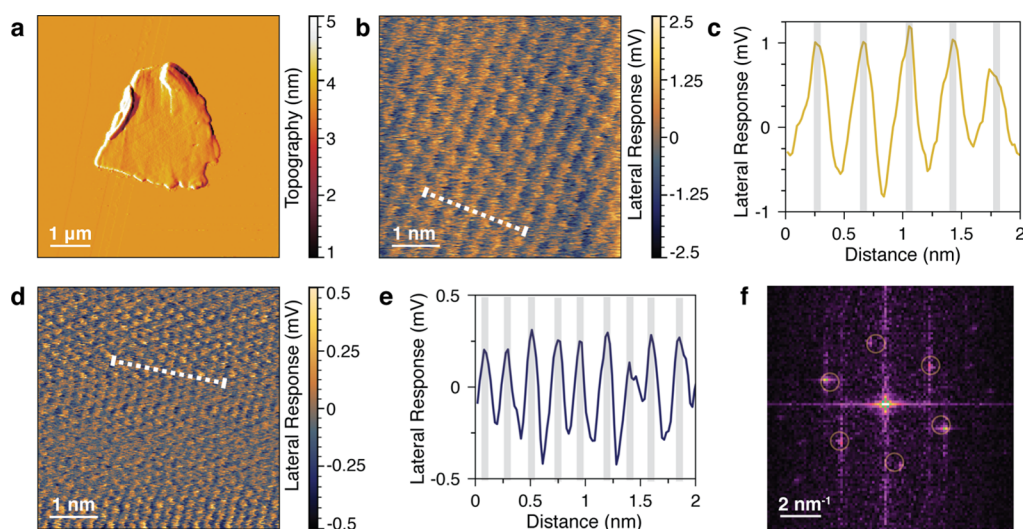


**Figure 4.** Scanning probe microscopy of a  $\gamma$ -graphyne flake. (a) AFM topography map of a  $\gamma$ -graphyne flake. (b,d) Lateral deflection maps of a region of the  $\gamma$ -graphyne flake and the HOPG substrate control in (a). (c,e) Plots of lateral response along the linear traces from (b) and (d). Gray bars mark the confidence interval for lattice constants. (f) FFT of the map from (b). Circles highlight the periodicity for the (2110) planes of  $\gamma$ -graphyne from electron diffraction (Figure 3b).

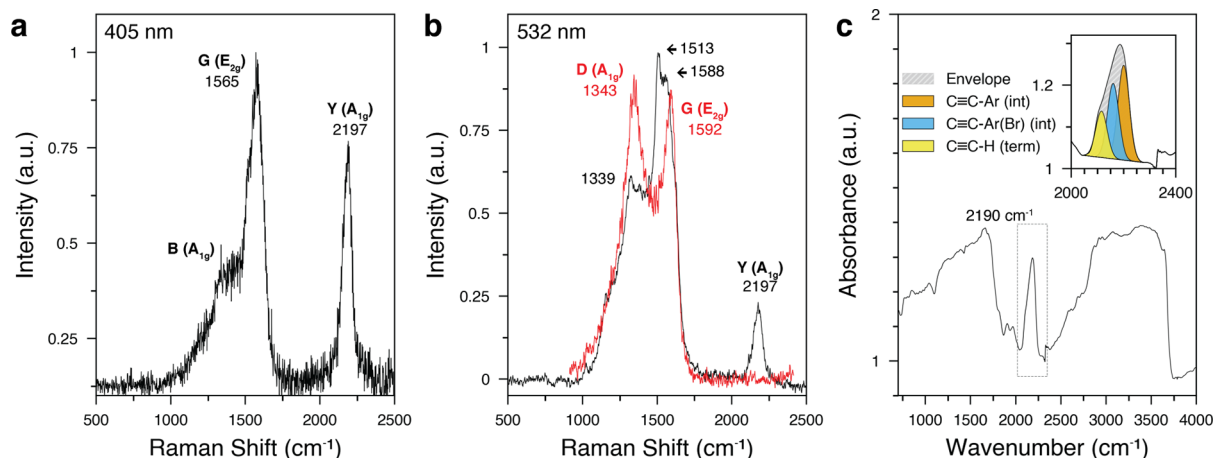


**Figure 5.** Vibrational spectroscopy of  $\gamma$ -graphyne. (a) Raman spectrum of  $\gamma$ -graphyne measured using an excitation wavelength of 405 nm (4.3 mW). (b) Raman spectra of  $\gamma$ -graphyne measured using an excitation wavelength of 532 nm. Black trace: <0.3 mW for less than 10 s. Red trace: <0.3 mW, after high-power irradiation at 7.5 mW for 30 s. (c) Mid-IR spectrum of polycrystalline  $\gamma$ -graphyne. Inset: deconvolution of the alkyne absorption peak at  $2190\text{ cm}^{-1}$ .

to yield the most symmetric spot intensity distribution, which corresponds to a beam normal to the basal plane and coincident with the  $a$  axis. Then, the sample was rotated around the  $b$  axis. As the sample rotation reached  $\sim 45^\circ$ , diffraction patterns that involve the  $z$  spacings began to appear. The experimental diffractograms in this orientation provided groups of closely spaced spots (Figure 3c), suggesting defects in the layer stacking. Such defects would not appear in the  $c$  orientation diffractograms, as the stacking mode only affects reflections involving  $z$  spacing (Figure S24, Supporting Information). The symmetry of the patterns agrees with our simulations for this intermediate orientation (Figure S23e,f,h, Supporting Information). As no systematic absences were observed, we can exclude some of the more symmetric space groups, most notably  $P6_3mc$ . The experimental diffraction patterns were most consistent with either one of the lower symmetry stacking modes, such as  $P3_112$  (Figure S22e, Supporting Information), or an aperiodic superlattice. It is important to note that despite their multispot character, the

observed diffractograms are not indicative of turbostratic stacking, which would produce ring patterns. The shape factor effect alters the geometry of the diffracted beam,<sup>34</sup> which introduces error into the determination of spot centers. Although this prohibits the precise measurement of interplanar spacings, the simulations indicate that the interlayer spacing estimated from SAED agrees with our PXRD data (Figure S23, Supporting Information).

We further probed the structure of  $\gamma$ -graphyne flakes by using lateral force microscopy (LFM). LFM is a technique closely related to contact-mode atomic force microscopy (AFM). In LFM, the scanning tip is rastered across the surface of the sample while maintaining contact, and the torsional moment due to stick-slip friction is measured. LFM can achieve resolution approaching that of scanning tunneling microscopy (STM),<sup>35</sup> which is often the technique of choice for the direct imaging of atomic arrangements. However, STM cannot be usefully applied to our sample due to the presence of adsorbates that roughen its surface. In contrast, lattice-

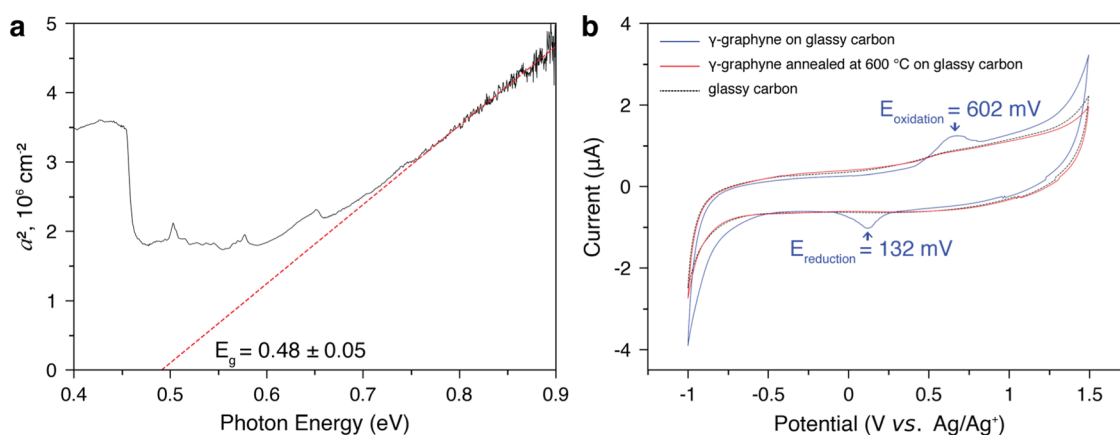


**Figure 6.** Electronic properties of  $\gamma$ -graphyne. (a) Determination of the optical band gap from the near-IR spectrum of polycrystalline  $\gamma$ -graphyne. (b) Cyclic voltammetry of  $\gamma$ -graphyne powder on glassy carbon. These are three-electrode measurements in 0.1 M  $n$ -Bu<sub>4</sub>N-PF<sub>6</sub>/acetonitrile-supporting electrolyte, with Pt counter electrode and an Ag/AgNO<sub>3</sub> (0.1 M) reference electrode at a scan rate of 50 mV/s.

resolution LFM imaging can often be performed even on rough substrates under ambient conditions.<sup>36</sup> We prepared a sample for imaging by ultrasonically dispersing the  $\gamma$ -graphyne flakes in water and casting them on a freshly cleaved surface of highly oriented pyrolytic graphite (HOPG). A lateral deflection map for a flat region of one of the  $\gamma$ -graphyne flakes (Figure 4a,b) was then recorded. In the same imaging session, with the same tip, we then obtained a lateral deflection map of the underlying HOPG as a reference (Figure 4d). Fast Fourier transforms (FFT) of LFM images of both the  $\gamma$ -graphyne flake and HOPG showed hexagonal arrangements of high-intensity spots, indicating the hexagonal symmetry for both lattices (Figure S27b,c, Supporting Information). The periodicity of  $\sim 2.4$  Å observed for the HOPG lattice (Figures 4e, S26, and S27c, Supporting Information) agrees with the expected value.<sup>35</sup> The lattice of the  $\gamma$ -graphyne flake is visibly less dense (Figure 4c). Its periodicity of  $\sim 3.4$  Å (one-half of the  $a$ -axis spacing) agrees with the theoretically predicted distance between the (1120) planes of  $\gamma$ -graphyne, which is also observed as a second-order reflection in electron diffraction (Figures 3b,d, and 4f).

The observed Raman spectra are consistent with expectations for  $\gamma$ -graphyne.<sup>37,38</sup> The distinctive Y ( $A_{1g}$ ) band corresponding to the C $\equiv$ C stretch of internal triple bonds appears at 2197 cm<sup>-1</sup> (Figure 5a). The G band, which corresponds to the  $E_{2g}$  modes of the aromatic rings, is centered at 1565 cm<sup>-1</sup>, exhibiting the predicted softening<sup>37</sup> relative to the G bands of common graphitic materials ( $\sim 1580$  cm<sup>-1</sup>) due to the additional resonant configurations from the  $\pi$ -electron delocalization along the acetylenic linkages.<sup>39</sup> A broad D band, corresponding to  $A_{1g}$  breathing of aromatic rings, is observed at  $\sim 1350$  cm<sup>-1</sup> and is expected to be sensitive to the domain size, lattice defects, and the excitation wavelength. A broad survey scan (500–3000 cm<sup>-1</sup>) showed no other Raman features for the 405 nm excitation wavelength, most notably no C–H stretches (2800–3000 cm<sup>-1</sup>) or the Y' band at  $\sim 1900$  cm<sup>-1</sup> characteristic of diacetylenes.<sup>29</sup> In the spectra of the TBTEB monomer (Figure S32, Supporting Information), a band at 2114 cm<sup>-1</sup>, corresponding to the stretch of the terminal C $\equiv$ C–H triple bonds, is observed. This band is not seen in the spectra of  $\gamma$ -graphyne, most likely due to the low ratio of terminal to internal triple bond sites.

It is important to note that our attempts to obtain the Raman spectra of  $\gamma$ -graphyne using 532 nm excitation, for incident power above 0.75 mW using a 0.55 NA 50 $\times$  objective,

resulted in a rapid and irreversible transformation of the material. This transformation was marked by the bleaching of the Y band, the increase in the intensity of the D band, and the shift of the G band to  $\sim 1590$  cm<sup>-1</sup> (Figure 5b). The resulting Raman signature is similar to that of disordered graphitic carbons.<sup>40</sup> The transformation is not due to direct oxidation, as experiments conducted in air and under  $\sim 1 \times 10^{-3}$  mbar vacuum resulted in similar observations.  $\gamma$ -Graphyne retains its characteristic Raman signature under prolonged high-power 405 nm illumination ( $>4$  mW), while rapidly transforming under 532 nm laser light (Figure S28c, Supporting Information), which suggests a photochemical process. Under stable low-power 532 nm illumination ( $<0.3$  mW), the degree of transformation does not linearly correlate with the exposure dose (Figure S28a,b, Supporting Information), suggesting thresholding photochemical behavior. A plausible pathway of the transformation involves Masamune–Bergman cycloaromatization, which has been demonstrated for a single 12-DBA subunit on a copper surface.<sup>41</sup> The observed splitting of the G band under 532 nm excitation, but not 405 nm excitation (black trace, Figure 5b), is not yet well understood and could be due to partial transformation from the 532 nm light even when measured at a relatively low excitation intensity.

The micro-Fourier transform infrared (FTIR) spectra of polycrystalline flakes of  $\gamma$ -graphyne featured wide-band absorption in the fingerprint region, as well as between 2800 and 3700 cm<sup>-1</sup> (Figure 5c). Absorption in these regions is associated with the vibrations of the aromatic rings of  $\gamma$ -graphyne, as well as contributions from the C–H and O–H groups on the periphery of the sheets or belonging to adventitious small-molecule adsorbates. The distorted line shape of these bands, as well as the change in line shape observed for the flakes of different thicknesses, suggests significant contribution from resonant Mie scattering.<sup>42,43</sup> Thus, we could not identify specific vibration frequencies or their true intensities for low- and high-frequency mid-IR regions. However, a distinctive peak corresponding to acetylenic bonds centered at  $\sim 2190$  cm<sup>-1</sup> was observed in the mid-IR-silent region (1700–2500 cm<sup>-1</sup>). As the C $\equiv$ C stretch is IR-inactive for symmetric alkynes, an ideal infinite monolayer of  $\gamma$ -graphyne would not possess this band. However, symmetry-breaking due to stacking of graphyne sheets, as well as finite and defective sheets, could activate this

absorption, as for the appearance of the D band in the Raman spectra of milled graphite.<sup>44</sup> The IR absorption reveals a prominent low-frequency shoulder (Figure 5c, inset), due to the contribution of the terminal alkyne species at the sheet edges (C≡C–H stretch, ~2115 cm<sup>-1</sup>).

The near-IR absorbance spectrum of  $\gamma$ -graphyne shows a strong onset of the fundamental electronic edge at high frequencies (5000–7500 cm<sup>-1</sup>), which is manifested as a monotonic decrease of absorbance with respect to frequency and as an optical phonon fingerprint in the infrared shoulder (Figure 6a). The dependence of absorbance on photon energy within the electronic edge can be used to estimate the electronic band gap,  $E_g$ , and determine the type of semiconductor. The absorption coefficient  $\alpha$  is defined as  $\alpha = (1/x) \times \ln(1/T)$ , where  $x$  is the sample thickness and  $T$  is transmittance, the ratio of transmitted to incident light intensity. Within the semiclassical theory of the optical absorption of crystalline direct band gap semiconductors,  $\alpha(E)$  is expected to be 0 for  $E < E_g$  and proportional to  $(E - E_g)^{1/2}$  for  $E \geq E_g$ .<sup>45,46</sup> Thus,  $E_g$  can be estimated by plotting  $\alpha^2$  versus  $E$  and extrapolating the linear region of the curve to the energy axis (Figure 6a). This  $\alpha^2$  versus  $E$  plot gives an optical band gap of  $E_g = 0.48 \pm 0.05$  eV for  $\gamma$ -graphyne, where the uncertainty indicates the standard deviation for over 20 polycrystalline particles.

To investigate the redox properties of  $\gamma$ -graphyne, a working electrode was prepared by ultrasonically dispersing 1 mg of  $\gamma$ -graphyne in 1 mL of a 1:1 v/v mixture of ethanol and water and then casting this suspension onto a glassy carbon electrode with subsequent air drying. Three-electrode cyclic voltammetry (CV) measurements were then conducted in acetonitrile with *n*-Bu<sub>4</sub>N·PF<sub>6</sub> supporting electrolyte for potentials between -1.0 and +1.5 V versus Ag/Ag<sup>+</sup> (0.1 M). An oxidation peak at 602 mV and a reduction peak at 132 mV were observed (Figure 6b, blue trace), corresponding to an electrochemical band gap of 0.47 eV.<sup>47</sup> This value agrees with the band gap determined by the optical absorption measurements.

To evaluate thermal stability,  $\gamma$ -graphyne particles were supported over holes in thin mica films by single-layer carbon nanotube sheets and then heated to gradually increasing set points under vacuum ( $1.3 \times 10^{-3}$  mbar). After 1 h at the set temperature, the sample assembly was cooled down and transferred to an FTIR microscope for analysis. The same sample region was analyzed for consistency. Heating up to 240 °C did not produce any major changes in the FTIR spectra beyond a slight decrease in the intensity of the 2800–3700 cm<sup>-1</sup> band, likely due to the removal of adventitious adsorbates (Figure S30a, Supporting Information). Loss of the alkyne band at 2100–2200 cm<sup>-1</sup> was observed at just over 240 °C, suggesting an onset of a structural transformation. The material lost all the alkyne absorbance after the 1 h thermal cycling processes reached 350 °C (Figure S30b, Supporting Information). The absorbance shoulder corresponding to terminal alkynes disappeared before the internal alkyne components of the band. The loss of alkyne absorption was accompanied by the disappearance of the Mie scattering bands in the fingerprint region and the region between 2800 and 3700 cm<sup>-1</sup>, suggesting a significant rearrangement of the microcrystalline structure. The material annealed to 600 °C lost the characteristic reduction and oxidation peaks in CV, indicating a major chemical change (Figure 6b, red trace). Despite the dramatic transformation of the IR signature, the optical images of the thermally treated samples revealed no

major textural or geometric changes on heating up to 450 °C (Figure S30c, Supporting Information). Due to its sensitivity to the different alkyne bonds present in the sample, the IR absorbance was found to be a useful marker for monitoring the structural changes of  $\gamma$ -graphyne.

Our data indicate that the material we synthesized is multilayer  $\gamma$ -graphyne. Contrary to expectations, we found that no external template is required for synthesizing highly crystalline  $\gamma$ -graphyne. There is no experimental evidence even in our reactions performed with Cu foil that any polymerization is happening on the surface. The lower crystallinity of the products obtained in the presence of Cu foil is likely due to the reduced concentration of catalytic Cu species in solution. This results in slower Sonogashira coupling and a higher extent of side reactions compared to the homogeneous Pd(PPh<sub>3</sub>)<sub>4</sub>/CuI protocol.

We tried to understand why TBTEB preferentially polymerizes into multilayer  $\gamma$ -graphyne flakes, as opposed to amorphous branched structures. As the polymerization appears to be self-templating, we assumed the existence of an attractive supramolecular interaction between TBTEB and the lattice of  $\gamma$ -graphyne. Self-assembly through solvophobicity driven  $\pi$ -stacking has been documented for several phenylene ethynylene oligomers and macrocycles structurally related to graphynes.<sup>48</sup> To explore the potential supramolecular interactions in our system, we computed by DFT the structure and potential energy surface for a single TBTEB molecule bound to a  $\gamma$ -graphyne monolayer. Our calculations predict that TBTEB would associate with the surface of graphyne at two types of binding sites (around the aromatic rings and over 12-DBA rings), with a binding energy in excess of 20 kcal/mol (Figure S33, Supporting Information). The monomer species outcompetes toluene, whose binding energy we estimate as ~11 kcal/mol. If every TBTEB species were to react while bound over the underlying layer of  $\gamma$ -graphyne, one of the many local energy minimum stackings or a mixture of the stackings could result.

## CONCLUSIONS

To our knowledge, our synthesis of  $\gamma$ -graphyne is the first example of an ordered covalent lattice formed spontaneously under purely kinetic control. Typical covalent organic frameworks and metal–organic frameworks are held together through bonds that are reversible. This reversibility is considered critical for continuous error correction during the reaction/crystallization process.<sup>49</sup> Conventional thinking predicts that irreversible polymerization of an A<sub>3</sub>B<sub>3</sub>-type monomer, not employing a strict geometric constraint on reactivity, must yield only disordered branched structures. However, as we routinely observed micron-scale  $\gamma$ -graphyne crystallites, 2D polymerization assisted by crystallization must be presently kinetically favored over random 3D growth. Furthermore, the initial nucleation of flat graphyne sheets appears to be a highly probable event. The high fidelity of the resulting lattices indicates that the system is capable of correcting errors despite the irreversibility of Sonogashira coupling. At a minimum, the reaction must proceed comparably well at both lattice edges and internal defect sites. As “patching” a single internal defect requires forming six new chemical bonds, it is highly likely that these bond-making steps are kinetically coupled. The apparent capability for error correction, as well as the strong dependence of the product structure on the nature of the Pd precatalyst, strongly

corroborates our original hypothesis of a multisite coupling mechanism.

Similar cross-coupling methodology could conceivably be applied to the synthesis of other graphyne-family allotropes, as well as to the theoretically proposed heteroatom-doped derivatives.<sup>50</sup> Performing the reaction at interfaces may provide access to extended few-layer or monolayer sheets rather than microcrystalline powders. These extended sheets could form the basis of the first  $\gamma$ -graphyne-based devices, especially as we observe a small, direct band gap. Further exploration of the chemical and physical properties of  $\gamma$ -graphyne is under way in our laboratories.

## ■ ASSOCIATED CONTENT

### SI Supporting Information

The Supporting Information is available free of charge at <https://pubs.acs.org/doi/10.1021/jacs.2c06583>.

Materials and methods; experimental procedures; NMR and FT-IR spectra; crystallographic information for the possible stacking modes of  $\gamma$ -graphyne sheets; supplemental figures and discussion referred to in the text; and computational data (PDF)

Models of the possible stacking modes of  $\gamma$ -graphyne sheets (ZIP)

## ■ AUTHOR INFORMATION

### Corresponding Author

**Valentin O. Rodionov** – Department of Macromolecular Science and Engineering, Case Western Reserve University, Cleveland, Ohio 44106, United States; [orcid.org/0000-0002-8293-0310](https://orcid.org/0000-0002-8293-0310); Email: [vor2@case.edu](mailto:vor2@case.edu)

### Authors

**Victor G. Desyatkin** – Department of Macromolecular Science and Engineering, Case Western Reserve University, Cleveland, Ohio 44106, United States

**William B. Martin** – Department of Macromolecular Science and Engineering, Case Western Reserve University, Cleveland, Ohio 44106, United States

**Ali E. Aliev** – Alan G. MacDiarmid NanoTech Institute, University of Texas at Dallas, Richardson, Texas 75080, United States; [orcid.org/0000-0003-0034-9707](https://orcid.org/0000-0003-0034-9707)

**Nathaniel E. Chapman** – Department of Macromolecular Science and Engineering, Case Western Reserve University, Cleveland, Ohio 44106, United States

**Alexandre F. Fonseca** – Applied Physics Department, Institute of Physics “Gleb Wataghin”, University of Campinas, Campinas, São Paulo 13083-970, Brazil; [orcid.org/0000-0001-8413-9744](https://orcid.org/0000-0001-8413-9744)

**Douglas S. Galvão** – Applied Physics Department, Institute of Physics “Gleb Wataghin”, University of Campinas, Campinas, São Paulo 13083-970, Brazil; [orcid.org/0000-0003-0145-8358](https://orcid.org/0000-0003-0145-8358)

**Ericka Roy Miller** – Department of Chemistry, Case Western Reserve University, Cleveland, Ohio 44106, United States

**Kevin H. Stone** – Stanford Synchrotron Radiation Lightsource, SLAC National Accelerator Laboratory, Menlo Park, California 94025, United States; [orcid.org/0000-0003-1387-1510](https://orcid.org/0000-0003-1387-1510)

**Zhong Wang** – Alan G. MacDiarmid NanoTech Institute, University of Texas at Dallas, Richardson, Texas 75080, United States; [orcid.org/0000-0002-1454-0601](https://orcid.org/0000-0002-1454-0601)

**Dante Zakhidov** – Department of Materials Science and Engineering, Stanford University, Stanford, California 94305, United States; [orcid.org/0000-0003-3107-104X](https://orcid.org/0000-0003-3107-104X)

**F. Ted Limpoco** – Oxford Instruments Asylum Research, Santa Barbara, California 93117, United States

**Sarah R. Almahdali** – Department of Macromolecular Science and Engineering, Case Western Reserve University, Cleveland, Ohio 44106, United States

**Shane M. Parker** – Department of Chemistry, Case Western Reserve University, Cleveland, Ohio 44106, United States; [orcid.org/0000-0002-1110-3393](https://orcid.org/0000-0002-1110-3393)

**Ray H. Baughman** – Alan G. MacDiarmid NanoTech Institute, University of Texas at Dallas, Richardson, Texas 75080, United States; [orcid.org/0000-0001-5845-5137](https://orcid.org/0000-0001-5845-5137)

Complete contact information is available at:

<https://pubs.acs.org/doi/10.1021/jacs.2c06583>

### Author Contributions

<sup>V</sup>V.G.D. and W.B.M. contributed equally.

### Notes

The authors declare no competing financial interest.

## ■ ACKNOWLEDGMENTS

The authors are grateful to Prof. Jessica Bickel (Cleveland State University) for discussions of scanning probe microscopy data. The authors thank the US Department of Energy (R01AB123456) and the National Science Foundation (GFRP award 1451075 to W.B.M.) for funding. R.H.B. acknowledges support from Robert A. Welch Foundation (grant AT-0029). D.S.G. and A.F.F. acknowledge support from São Paulo Research Foundation (FAPESP, awards #2013/08293-7 and #2020/02044-9), National Council for Scientific and Technological Development (CNPq), and the John David Rogers Computing Center (CCJDR) at the Institute of Physics “Gleb Wataghin”, University of Campinas. The authors thank Oxford Instruments Asylum Research for providing access to Cypher VRS AFM instrument. This work made use of the High Performance Computing Resource in the Core Facility for Advanced Research Computing at Case Western Reserve University. Raman spectroscopy was performed at the Stanford Nano Shared Facilities (SNSF), supported by the National Science Foundation under award ECCS-2026822. The use of the Stanford Synchrotron Radiation Lightsource, SLAC National Accelerator Laboratory, was supported by the U.S. Department of Energy, Office of Science, Office of Basic Energy Sciences, under contract DE-AC02-76SF00515.

## ■ REFERENCES

- (1) Hoffmann, R.; Kabanov, A. A.; Golov, A. A.; Proserpio, D. M. Homo Citans and Carbon Allotropes: For an Ethics of Citation. *Angew. Chem., Int. Ed.* **2016**, *55*, 10962–10976.
- (2) Geim, A. K.; Novoselov, K. S. The rise of graphene. *Nat. Mater.* **2007**, *6*, 183–191.
- (3) Baughman, R. H.; Zakhidov, A. A.; de Heer, W. A. Carbon nanotubes—the route toward applications. *Science* **2002**, *297*, 787–792.
- (4) Wudl, F. Fullerene materials. *J. Mater. Chem.* **2002**, *12*, 1959–1963.
- (5) Liu, J.; Mishra, S.; Pignedoli, C. A.; Passerone, D.; Urgel, J. I.; Fabrizio, A.; Lohr, T. G.; Ma, J.; Komber, H.; Baumgarten, M.; et al. Open-Shell Nonbenzenoid Nanographenes Containing Two Pairs of Pentagonal and Heptagonal Rings. *J. Am. Chem. Soc.* **2019**, *141*, 12011–12020.

- (6) Hieulle, J.; Carbonell-Sanromà, E.; Vilas-Varela, M.; Garcia-Lekue, A.; Guitián, E.; Peña, D.; Pascual, J. I. On-Surface Route for Producing Planar Nanographenes with Azulene Moieties. *Nano Lett.* **2018**, *18*, 418–423.
- (7) Fan, Q.; Yan, L.; Tripp, M. W.; Krejčí, O.; Dimosthenous, S.; Kachel, S. R.; Chen, M.; Foster, A. S.; Koert, U.; Liljeroth, P.; et al. Biphenylene network: A nonbenzenoid carbon allotrope. *Science* **2021**, *372*, 852–856.
- (8) Baughman, R. H. Chemistry. Dangerously seeking linear carbon. *Science* **2006**, *312*, 1009–1110.
- (9) Shi, L.; Rohringer, P.; Suenaga, K.; Niimi, Y.; Kotakoski, J.; Meyer, J. C.; Peterlik, H.; Wanko, M.; Cahangirov, S.; Rubio, A.; et al. Confined linear carbon chains as a route to bulk carbyne. *Nat. Mater.* **2016**, *15*, 634–639.
- (10) Baughman, R. H.; Eckhardt, H.; Kertesz, M. Structure-property predictions for new planar forms of carbon: Layered phases containing  $sp^2$  and  $sp$  atoms. *J. Chem. Phys.* **1987**, *87*, 6687–6699.
- (11) Kang, J.; Wei, Z.; Li, J. Graphyne and Its Family: Recent Theoretical Advances. *ACS Appl. Mater. Interfaces* **2019**, *11*, 2692–2706.
- (12) Zhang, H.; Zhao, M.; He, X.; Wang, Z.; Zhang, X.; Liu, X. High Mobility and High Storage Capacity of Lithium in  $sp$ - $sp^2$  Hybridized Carbon Network: The Case of Graphyne. *J. Phys. Chem. C* **2011**, *115*, 8845–8850.
- (13) Gao, X.; Liu, H.; Wang, D.; Zhang, J. Graphdiyne: synthesis, properties, and applications. *Chem. Soc. Rev.* **2019**, *48*, 908–936.
- (14) Wu, W.; Guo, W.; Zeng, X. C. Intrinsic electronic and transport properties of graphyne sheets and nanoribbons. *Nanoscale* **2013**, *5*, 9264–9276.
- (15) Chen, J.; Xi, J.; Wang, D.; Shuai, Z. Carrier Mobility in Graphyne Should Be Even Larger than That in Graphene: A Theoretical Prediction. *J. Phys. Chem. Lett.* **2013**, *4*, 1443–1448.
- (16) Wang, X. M.; Mo, D. C.; Lu, S. S. On the thermoelectric transport properties of graphyne by the first-principles method. *J. Chem. Phys.* **2013**, *138*, 204704.
- (17) Zhang, Y. Y.; Pei, Q. X.; Wang, C. M. Mechanical properties of graphynes under tension: A molecular dynamics study. *Appl. Phys. Lett.* **2012**, *101*, 081909.
- (18) Haley, M. M. Synthesis and properties of annulenic subunits of graphyne and graphdiyne nanoarchitectures. *Pure Appl. Chem.* **2008**, *80*, 519–532.
- (19) Diederich, F.; Kivala, M. All-carbon scaffolds by rational design. *Adv. Mater.* **2010**, *22*, 803–812.
- (20) Gao, X.; Zhu, Y.; Yi, D.; Zhou, J.; Zhang, S.; Yin, C.; Ding, F.; Zhang, S.; Yi, X.; Wang, J.; et al. Ultrathin graphdiyne film on graphene through solution-phase van der Waals epitaxy. *Sci. Adv.* **2018**, *4*, No. eaat6378.
- (21) Gao, H. Y.; Wagner, H.; Zhong, D.; Franke, J. H.; Studer, A.; Fuchs, H. Glaser coupling at metal surfaces. *Angew. Chem., Int. Ed. Engl.* **2013**, *52*, 4024–4028.
- (22) Chinchilla, R.; Nájera, C. The Sonogashira reaction: a booming methodology in synthetic organic chemistry. *Chem. Rev.* **2007**, *107*, 874–922.
- (23) Eickmeier, C.; Junga, H.; Matzger, A. J.; Scherhag, F.; Shim, M.; Vollhardt, K. P. C. 5,6,11,12,17,18-Hexadehydro-1,4,7,10,13,16-hexaethynyltribenzo[a,e,i]cyclododecene: Synthesis and CpCo-Catalyzed Cycloisomerization to the First Superdelocalized Oligophenylenes. *Angew. Chem., Int. Ed. Engl.* **1997**, *36*, 2103–2108.
- (24) Larrosa, I.; Somoza, C.; Banquy, A.; Goldup, S. M. Two Flavors of PEPPSI-IPr: Activation and Diffusion Control in a Single NHC-Ligated Pd Catalyst? *Org. Lett.* **2011**, *13*, 146–149.
- (25) Xue, Z.; Finke, A. D.; Moore, J. S. Synthesis of Hyperbranched Poly(m-phenylene)s via Suzuki Polycondensation of a Branched  $AB_2$  Monomer. *Macromolecules* **2010**, *43*, 9277–9282.
- (26) Sakamoto, J.; Rehahn, M.; Wegner, G.; Schlüter, A. D. Suzuki Polycondensation: Polyarylenes a la Carte. *Macromol. Rapid Commun.* **2009**, *30*, 653–687.
- (27) Díez-González, S. Copper(I)-Acetylides. In *Advances in Organometallic Chemistry*; Pérez, P. J., Ed.; Advances in Organometallic Chemistry; Academic Press, 2016; Vol. 66, pp 93–141.
- (28) Rossi, S.; Bisello, A.; Cardena, R.; Orian, L.; Santi, S. Benzodithiophene and Benzotrithiophene as  $\pi$  Cores for Two- and Three-Blade Propeller-Shaped Ferrocenyl-Based Conjugated Systems. *Eur. J. Org. Chem.* **2017**, *2017*, 5966–5974.
- (29) Matsuoka, R.; Sakamoto, R.; Hoshiko, K.; Sasaki, S.; Masunaga, H.; Nagashio, K.; Nishihara, H. Crystalline Graphdiyne Nanosheets Produced at a Gas/Liquid or Liquid/Liquid Interface. *J. Am. Chem. Soc.* **2017**, *139*, 3145–3152.
- (30) Iucci, G.; Carravetta, V.; Altamura, P.; Russo, M. V.; Paolucci, G.; Goldoni, A.; Polzonetti, G. XPS, NEXAFS and theoretical study of phenylacetylene adsorbed on Cu(100). *Chem. Phys.* **2004**, *302*, 43–52.
- (31) Beamson, G.; Briggs, D. *High Resolution XPS of Organic Polymers: The Scienta ESCA300 Database*; Wiley, 1992.
- (32) Ducéré, J.-M.; Lepetit, C.; Chauvin, R. Carbo-graphite: Structural, Mechanical, and Electronic Properties. *J. Phys. Chem. C* **2013**, *117*, 21671–21681.
- (33) Williams, D. B.; Carter, C. B. Obtaining and Indexing Parallel-Beam Diffraction Patterns. In *Transmission Electron Microscopy*; Springer, 2009; pp 283–309.
- (34) Thomas, G.; Goringe, M. J. *Transmission Electron Microscopy of Materials*; Wiley, 1979.
- (35) Mate, C. M.; McClelland, G. M.; Erlandsson, R.; Chiang, S. Atomic-scale friction of a tungsten tip on a graphite surface. *Phys. Rev. Lett.* **1987**, *59*, 1942–1945.
- (36) Marsden, A. J.; Phillips, M.; Wilson, N. R. Friction force microscopy: a simple technique for identifying graphene on rough substrates and mapping the orientation of graphene grains on copper. *Nanotechnology* **2013**, *24*, 25S704.
- (37) Popov, V. N.; Lambin, P. Theoretical Raman fingerprints of  $\alpha$ -,  $\beta$ -, and  $\gamma$ -graphyne. *Phys. Rev. B: Condens. Matter Mater. Phys.* **2013**, *88*, 075427.
- (38) Zhang, S.; Wang, J.; Li, Z.; Zhao, R.; Tong, L.; Liu, Z.; Zhang, J.; Liu, Z. Raman Spectra and Corresponding Strain Effects in Graphyne and Graphdiyne. *J. Phys. Chem. C* **2016**, *120*, 10605–10613.
- (39) Exarhos, G. J.; Risen, W. M.; Baughman, R. H. Resonance Raman study of the thermochromic phase transition of a polydiacetylene. *J. Am. Chem. Soc.* **2002**, *98*, 481–487.
- (40) Ferrari, A. C.; Robertson, J. Resonant Raman spectroscopy of disordered, amorphous, and diamondlike carbon. *Phys. Rev. B* **2001**, *64*, 075414.
- (41) Kawai, S.; Haapasilta, V.; Lindner, B. D.; Tahara, K.; Spijker, P.; Buitendijk, J. A.; Pawlak, R.; Meier, T.; Tobe, Y.; Foster, A. S.; et al. Thermal control of sequential on-surface transformation of a hydrocarbon molecule on a copper surface. *Nat. Commun.* **2016**, *7*, 12711.
- (42) van Dijk, T.; Mayerich, D.; Carney, P. S.; Bhargava, R. Recovery of absorption spectra from Fourier transform infrared (FT-IR) microspectroscopic measurements of intact spheres. *Appl. Spectrosc.* **2013**, *67*, 546–552.
- (43) Bassan, P.; Byrne, H. J.; Bonnier, F.; Lee, J.; Dumas, P.; Gardner, P. Resonant Mie scattering in infrared spectroscopy of biological materials—understanding the ‘dispersion artefact’. *Analyst* **2009**, *134*, 1586–1593.
- (44) Xing, T.; Li, L. H.; Hou, L.; Hu, X.; Zhou, S.; Peter, R.; Petracic, M.; Chen, Y. Disorder in ball-milled graphite revealed by Raman spectroscopy. *Carbon* **2013**, *57*, 515–519.
- (45) Tauc, J.; Grigorovici, R.; Vancu, A. Optical Properties and Electronic Structure of Amorphous Germanium. *Phys. Status Solidi B* **1966**, *15*, 627–637.
- (46) Zanatta, A. R. Revisiting the optical bandgap of semiconductors and the proposal of a unified methodology to its determination. *Sci. Rep.* **2019**, *9*, 11225.

(47) Haram, S. K.; Quinn, B. M.; Bard, A. J. Electrochemistry of CdS nanoparticles: a correlation between optical and electrochemical band gaps. *J. Am. Chem. Soc.* **2001**, *123*, 8860–8861.

(48) Lahiri, S.; Thompson, J. L.; Moore, J. S. Solvophobicity Driven  $\pi$ -Stacking of Phenylene Ethynylene Macrocycles and Oligomers. *J. Am. Chem. Soc.* **2000**, *122*, 11315–11319.

(49) Kory, M. J.; Wörle, M.; Weber, T.; Payamyar, P.; van de Poll, S. W.; Dshemuchadse, J.; Trapp, N.; Schlüter, A. D. Gram-scale synthesis of two-dimensional polymer crystals and their structure analysis by X-ray diffraction. *Nat. Chem.* **2014**, *6*, 779–784.

(50) Zhou, J.; Lv, K.; Wang, Q.; Chen, X. S.; Sun, Q.; Jena, P. Electronic structures and bonding of graphyne sheet and its BN analog. *J. Chem. Phys.* **2011**, *134*, 174701.

## Recommended by ACS

### Dipole-Modulated Charge Transport through PNP-Type Single-Molecule Junctions

Mingyao Li, Xuefeng Guo, *et al.*

OCTOBER 23, 2022  
JOURNAL OF THE AMERICAN CHEMICAL SOCIETY

READ 

### Steering the Topological Defects in Amorphous Laser-Induced Graphene for Direct Nitrate-to-Ammonia Electroreduction

Le Cheng, Ruquan Ye, *et al.*

SEPTEMBER 09, 2022  
ACS CATALYSIS

READ 

### A Series of Soluble Thieno-Fused Coronene Nanoribbons of Precise Lengths

Xuan Yang, Michael Mastalerz, *et al.*

MAY 29, 2022  
JOURNAL OF THE AMERICAN CHEMICAL SOCIETY

READ 

### Nanographenes and Graphene Nanoribbons as Multitalents of Present and Future Materials Science

Yanwei Gu, Klaus Müllen, *et al.*

JUNE 07, 2022  
JOURNAL OF THE AMERICAN CHEMICAL SOCIETY

READ 

Get More Suggestions >